Acta Crystallographica Section D
Biological Crystallography
ISSN 0907-4449

Structure of Nm23-H1 under oxidative conditions

Mi-Sun Kim,[a]‡ Jaeho Jeong,[a,b]‡ Jihye Jeong,[a] Dong-Hae Shin[a]* and Kong-Joo Lee[a]*

[a]The Center for Cell Signaling and Drug Discovery Research, College of Pharmacy, Division of Life and Pharmaceutical Sciences, Ewha Womans University, Seoul 120-750, Republic of Korea, and [b]Graduate Program for Nanomedical Science, Yonsei University, Seoul 120-749, Republic of Korea

‡ These authors contributed equally to this work.

Correspondence e-mail: dhshin55@ewha.ac.kr, kjl@ewha.ac.kr

Received 26 October 2012
Accepted 11 January 2013

PDB Reference: oxidized Nm23-H1, 4eno

Nm23-H1/NDPK-A, a tumour metastasis suppressor, is a multifunctional housekeeping enzyme with nucleoside diphosphate kinase activity. Hexameric Nm23-H1 is required for suppression of tumour metastasis and it is dissociated into dimers under oxidative conditions. Here, the crystal structure of oxidized Nm23-H1 is presented. It reveals the formation of an intramolecular disulfide bond between Cys4 and Cys145 that triggers a large conformational change that destabilizes the hexameric state. The dependence of the dissociation dynamics on the H_2O_2 concentration was determined using hydrogen/deuterium-exchange experiments. The quaternary conformational change provides a suitable environment for the oxidation of Cys109 to sulfonic acid, as demonstrated by peptide sequencing using nanoUPLC-ESI-q-TOF tandem MS. From these and other data, it is proposed that the molecular and cellular functions of Nm23-H1 are regulated by a series of oxidative modifications coupled to its oligomeric states and that the modified cysteines are resolvable by NADPH-dependent reduction systems. These findings broaden the understanding of the complicated enzyme-regulatory mechanisms that operate under oxidative conditions.

1. Introduction

Under oxidative conditions, redox-active cysteines undergo oxidative modifications with the formation of disulfides and derivatives such as sulfenic, sulfinic and sulfonic acids (Reddie & Carroll, 2008). These modifications are closely involved in the regulatory functions of many enzymes. The highly reactive cysteines in these redox-regulated proteins recognize changes in the redox environment through disulfide bonds and quickly translate their structures into active or inactive conformations. As a consequence of disulfide formation, OxyR (Choi *et al.*, 2001) and Hsp33 (Janda *et al.*, 2004) are activated and RsrA (Zdanowski *et al.*, 2006) and IpaH9.8 E3 ligase (Seyedarabi *et al.*, 2010) are inactivated. The oxidation of a cysteine thiol to a sulfenic, sulfinic or sulfonic acid is known to inactivate peroxiredoxins (Hall *et al.*, 2009) and phosphatases (Montfort *et al.*, 2003). In contrast, these derivatives are essential for the proper function of matrix metalloproteases (Fu *et al.*, 2001) and nitrile hydratases (Nagashima *et al.*, 1998). Therefore, the regulation of enzyme functions through oxidative modification may be common in nature.

Nm23, a tumour metastasis suppressor, is a multifunctional housekeeping enzyme with nucleoside diphosphate kinase (NDPK; Wagner & Vu, 1995), histidine protein kinase (Freije *et al.*, 1997) and 3′–5′ exonuclease activities (Jarrett *et al.*,

2011). It is involved in the regulation of tumour metastasis, development, differentiation, proliferation, endocytosis and apoptosis (Berlett & Stadtman, 1997). There are at least eight known NDPK genes in the human genome (Ishikawa *et al.*, 2003) with the common NDPK domain (Fig. 1). Interestingly, the tumour metastasis suppressing activity of Nm23-H1 is correlated with its oligomeric state rather than its NDPK activity (Kim *et al.*, 2003). A conformational change in the K-pn loop region is known to induce the dissociation of a hexamer into dimers. In previous studies, we have reported that Cys109 is modified to various oxidation states such as glutathionylation and sulfonic acid in response to treatment with H_2O_2 (Lee *et al.*, 2009). Cys4 and Cys145 form a disulfide bond under oxidative conditions (Kim *et al.*, 2010). Interestingly, these modifications promote dissociation of Nm23-H1 from a hexamer into dimers (Song *et al.*, 2000). As a result, oxidized Nm23-H1 loses its tumour metastasis suppressor activity as well as its enzymatic activity.

We also observed that oxidized Nm23-H1 is a substrate of the NADPH–thioredoxin reductase 1–thioredoxin (NADPH–TrxR1–Trx) system and that disulfide cross-linking is recovered by this system (Lee *et al.*, 2009). However, the mechanism of the process of inactivation of Nm23-H1 by these oxidative modifications is not yet understood at the molecular level.

Currently, 65 NDPK homologue structures have been deposited in the Protein Data Bank (PDB). They share a core globular α/β domain with more than 30% sequence identity. However, the oligomeric structure varies depending on the organism. For example, a dimeric form was observed in *Halomonas* sp. 593 (Arai *et al.*, 2012), tetrameric forms in *Myxococcus xanthus* (Strelkov *et al.*, 1995) and *Escherichia coli* (Moynié *et al.*, 2007) and hexameric forms in *Dictyostelium discoideum* (Moréra *et al.*, 1994) and *Homo sapiens* (Min *et al.*, 2002).

A number of X-ray crystal structures are available for Nm23-H1, including native (Min *et al.*, 2002; Han *et al.*, 2010), single-mutant (Giraud *et al.*, 2006) and double-mutant (Chen *et al.*, 2003) forms. All form a hexamer with *D*3 symmetry and each subunit has a globular α/β domain with a ferredoxin-like fold and an extended C-terminal domain. The native form showed a difference from Nm23-H2 in electrostatic surface potential that influenced its DNA-binding properties (Min *et al.*, 2002). Han *et al.* (2010) suggested a putative role of the N-terminal residues in the 3′–5′ exonuclease activity based on the observation of the N-terminal 3_{10}-helix H1 in their new crystal form. Since Nm23-H1 was purified under reducing conditions in both cases, no oxidative modification was reported. The crystal structure of the S120G mutant found in several aggressive neuroblastomas indicated no significant changes compared with that of the wild type, implying that the mutation might affect other protein properties apart from the NDP kinase activity (Giraud *et al.*, 2006). Structural study of H118G/F60W complexed with ADP, Ca^{2+} and inorganic phosphate led to the proposal of the possibility of designing nucleotide analogues with different affinities depending on the kinase type (Chen *et al.*, 2003). However, none of the reported

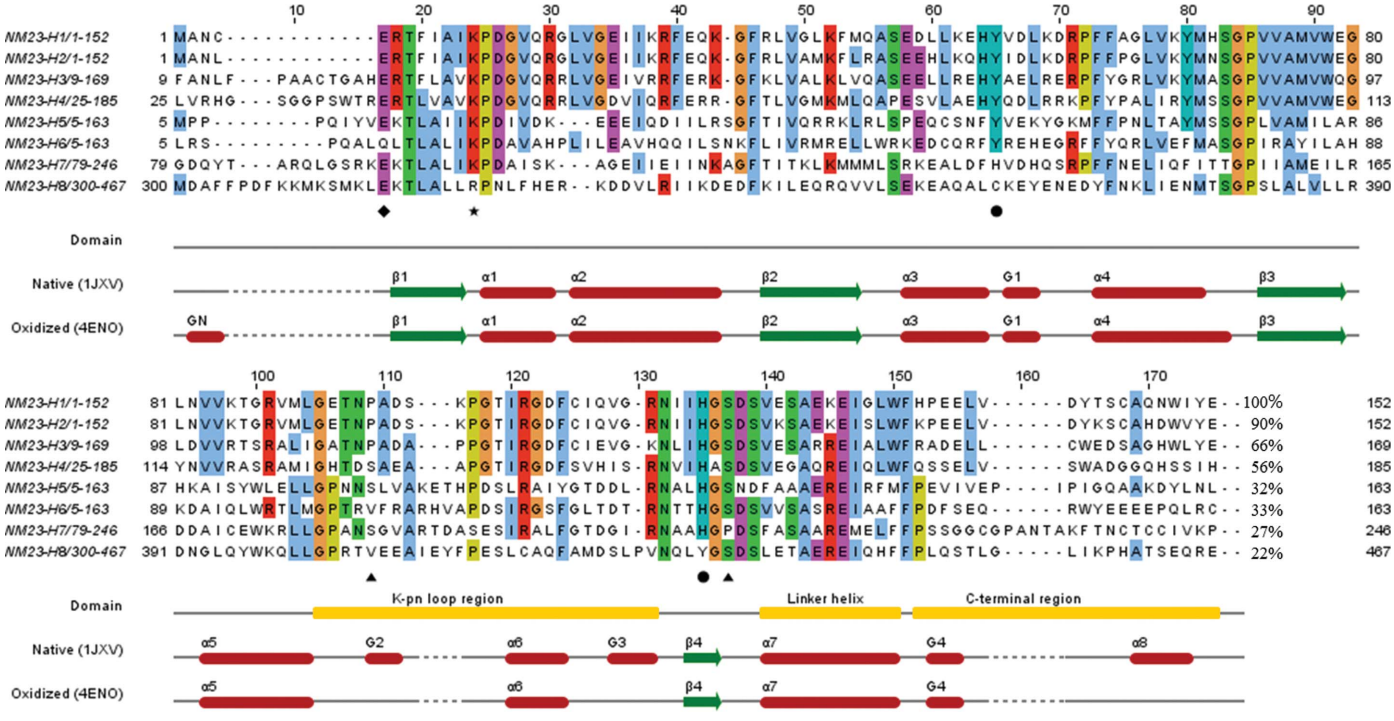

Figure 1
Sequence alignment of Nm23 family members. Consensus amino acids with more than 50% sequence identity are coloured according to the *ClustalX* colour scheme provided by the *Jalview* program (Waterhouse *et al.*, 2009). Sequence identities (%) of the Nm23 family members to Nm23-H1 are listed. Functionally important domains and secondary-structure elements are indicated below the sequence-alignment rows (α, α-helix; β, β-strand; G, 3_{10}-helix). The filled diamond indicates the key residue for 3′–5′ exonuclease activity, the filled circles those for both NDPK and histidine kinase activities and the filled star that for all three enzyme activities. The positions of Pro96 and Ser120 are indicated by filled triangles.

NDPK and Nm23-H1 structures were studied under oxidative conditions.

In order to identify the mechanism of the inactivation of Nm23-H1 by oxidative modifications, we have determined the crystal structure of oxidized Nm23-H1 followed by a series of biochemical experiments. Hydrogen/deuterium-exchange (HDX) experiments were also performed to identify the dissociation dynamics of oxidized Nm23-H1 from a hexamer into dimers. Based on these studies, we conclude that regulatory processes for the inactivation of Nm23-H1 through a series of oxidative modifications are coupled to its oligomeric state. In addition, this study helps to understand the structure–activity relationships of the known Nm23-H1 mutants at the atomic level.

2. Materials and methods

2.1. Materials

The sources of the various materials used in this study are as follows. Monoclonal anti-FLAG antibody (M2), deuterium oxide (D_2O; ≥99.9 atom% D) and other biochemicals including bis-acrylamide, TEMED, ammonium persulfate, sodium dodecyl sulfate (SDS), glycerol, glycine, β-mercaptoethanol and ATP-agarose were from Sigma (St Louis, Missouri, USA) and monoclonal anti-tubulin antibody was from Santa Cruz Biotechnology (Santa Cruz, California, USA). Eagles's minimum essential medium (EMEM) was from the American Type Culture Collection (ATCC; Manassas, Virginia, USA). Penicillin/streptomycin, foetal bovine serum and trypsin were from GIBCO Life Technologies Inc. (Grand Island, New York, USA). PEI cellulose TLC plates were from Altech (Deerfield, Illinois, USA) and sequencing-grade trypsin was from Promega (Fitchburg, Wisconsin, USA). [γ-^{32}P]ATP was from DuPont NENTM (Boston, Massachusetts, USA) and tris(2-carboxyethyl)phosphine hydrochloride (TCEP) was from Sigma–Aldrich (St Louis, Missouri, USA), trifluoroacetic acid (TFA), formic acid (FA) and HPLC-grade acetonitrile were from Merck (Darmstadt, Germany) and HPLC-grade water was from J. T. Baker.

2.2. Plasmids and protein purification

The expression plasmid pET-3c containing Nm23-H1 was provided by Dr P. S. Steeg at NCI, USA. For expression in mammalian cells, Nm23-H1 was cloned into the FLAG vector. *E. coli* strain BL21 (DE3) was used for protein expression. Recombinant protein was purified as described previously (Na *et al.*, 2008). Cytosolic fractions of *E. coli* strain BL21 (DE3) transformed with pET-3c expression plasmids containing the Nm23-H1 coding region were obtained after inducing the expression of each protein with 0.2 m*M* IPTG as described previously. Each cytosolic fraction was applied onto a 2–4 ml ATP Sepharose column equilibrated with buffer *A* (20 m*M* Tris–acetate, 20 m*M* NaCl, 0.1 m*M* EDTA, 3 m*M* $MgCl_2$ pH 7.4) at a flow rate of 3 ml min^{-1}. The column was washed with buffer *A* and then with buffer *A* containing 0.25 *M* NaCl to remove nonspecifically bound proteins. Nm23-H1 was then eluted with buffer *A* containing 1 m*M* ATP (Kim *et al.*, 1997).

2.3. NDPK activity assay

The enzymatic activity of Nm23-H1 was measured as reported previously (Song *et al.*, 2000). The enzyme was incubated in a 20 µl volume of reaction buffer *B* consisting of 20 m*M* HEPES pH 7.4, 0.1 m*M* ATP, 1 m*M* UDP as a substrate, 0.1 µCi [γ-^{32}P]ATP and 3 m*M* $MgCl_2$ for 10 min at 310 K. The reaction was stopped by adding gel-sample buffer consisting of 125 m*M* Tris base, 2.3% SDS, 10% glycerol. Aliquots were loaded onto PEI cellulose TLC plates and developed in 0.75 *M* KH_2PO_4 pH 3.6. The dried TLC plates were exposed for autoradiography and the formation of [γ-^{32}P]UTP was quantified using a Fuji Photo Film BAS 2000 (Tokyo, Japan). All measurements were performed in triplicate.

2.4. Sample preparation for mass spectrometry

Nm23-H1 was separated by gel electrophoresis and was detected by Coomassie Blue staining. The gel bands were excised with a scalpel, destained with 25 m*M* NH_4HCO_3/50% acetonitrile and washed to remove the destaining reagent. The pH was adjusted to 8.0 with 200 m*M* NH_4HCO_3 to facilitate trypsin digestion. The gels were dehydrated by the addition of acetonitrile, rehydrated by adding 10–20 µl 25 m*M* NH_4HCO_3 with 20 ng l^{-1} sequencing-grade trypsin (Promega Co.) and incubated at 310 K for 15–17 h. Peptides were extracted by adding 30 µl of a solution containing a gradient from 60% acetonitrile/0.1% TFA to 100% acetonitrile and the extracts were pooled and evaporated to dryness in a SpeedVac for MS analysis. Formic acid was added to the sample to a final concentration of 0.1% to facilitate electrospray ionization.

2.5. Peptide sequencing and quantification

Peptides were analyzed by nanoUPLC-ESI-q-TOF tandem MS (SYNAPT HDMS, Waters Co., UK). Peptides were separated using a C18 reversed-phase 75 µm internal diameter × 200 mm analytical column (1.7 mm particle size; BEH130 C18, Waters) with an integrated electrospray ionization PicoTip (±10 µm; New Objective, USA). 10 ml of peptide mixture was dissolved in 0.1%(*v*/*v*) formic acid in water, injected onto a column and eluted with a linear gradient of a 5–80% buffer containing 0.1%(*v*/*v*) formic acid in acetonitrile over 120 min. Samples were desalted online prior to separation using a trap column (180 µm internal diameter × 20 mm; Symmetry C18, Waters) cartridge. Initially, the flow rate was set to 300 nl min^{-1} and the capillary voltage (2.5 keV) was applied to the nanoUPLC mobile phase before spraying. Chromatography was performed online to the mass spectrometer. In the first run, the four most abundant precursors were selected for MS/MS analysis. Following positive identification, all peptides identified from a database search (*Mascot*) were nonredundantly excluded in the next run until full sequence coverage was obtained (Seo *et al.*, 2008).

Table 1
Refinement statistics.

Values in parentheses are for the highest resolution shell. The data were obtained from a single crystal.

PDB code	4eno
Statistics of the peak-wavelength MR data set	
Wavelength (Å)	1.000
Resolution (Å)	50.0–2.80 (2.95–2.80)
Multiplicity	15.3 (15.8)
Unique reflections	10205 (1457)
Completeness (%)	99.9 (100)
$\langle I/\sigma(I)\rangle$	4.1 (1.3)
$R_{\rm meas}$ (%)	17.9 (59.6)
Crystal parameters and refinement statistics	
Space group	$P2_13$
Unit-cell parameter (Å)	106.8
Solvent volume fraction (%)	56.4
$V_{\rm M}$ (Å^3 Da^{-1})	2.82
Total No. of residues	300
Total non-H atoms	2437
No. of phosphates	2
No. of water molecules	55
Average temperature factors (Å^2)	
Protein	27.71
Solvent	22.97
Phosphate	43.52
Resolution range of reflections used (Å)	19.83–2.80
Amplitude cutoff	0.0σ
R factor (%)	18.2 (24.5)
Free R factor (%)	25.6 (34.9)
Stereochemical ideality	
Bonds (Å)	0.009
Angles (°)	1.315
Chirality (°)	0.097
Planarity (°)	0.005
Dihedral (°)	17.05
Ramachandran plot, residues in (%)	
Most favoured regions	90.6
Additional allowed regions	9.1
Generously allowed regions	0.4
Disallowed regions	0.0

The individual MS/MS spectra acquired for each of the precursors within a single LC run were combined, smoothed, deisotoped and centroided using the Micromass *ProteinLynx Global Server* (*PLGS*) 2.3 data-processing software and were output as a single *Mascot*-searchable peak list (`.pkl`) file. The peak-list files were used to query the Swiss-Prot database using *Mascot* (global search engine) and *MOD*^{i} (http://prix.hanyang.ac.kr/modi/), with the following parameters: peptide mass tolerance 0.2 Da, MS/MS ion mass tolerance 0.2 Da and allowing up to one missed trypsin cleavage site. A large number of types of potential PTMs were considered. All reported assignments were verified by automatic and manual interpretation of spectra from *Mascot* and *MOD*^{i} in a blind mode (Kim *et al.*, 2006; Na *et al.*, 2008).

In order to quantify the oxidation of Cys109 in the wild type and the C4S and C145S mutants, the degree of oxidation to sulfonic acid at Cys109 was measured using mass spectrometry. Chromatograms of sulfonic acid and *N*-ethylmaleimide (NEM) labelled at Cys109 in the wild type and each mutant were extracted and the area ratios were calculated. To normalize the calculated ratio from different runs, 100 fmol GFP (Glu-fibrino peptide) was spiked as an internal standard peptide prior to each sample run.

2.6. HDX using mass spectrometry

Nm23-H1 was diluted tenfold with labelling buffer (20 m*M* PBS in D_2O pH 7.4) and maintained at 298 K with varying concentrations of H_2O_2. The labelling reaction was quenched with 5 m*M* TCEP pH 2.3 (titrated with formic acid). For peptic digestion, porcine pepsin (1 mg ml^{-1}) was added to each quenched protein sample and incubated at 273 K for 3 min before injection (Hoofnagle *et al.*, 2004).

Deuterated peptic peptides were desalted online prior to separation using a trap column (180 µm internal diameter × 20 mm; Symmetry C18) cartridge. Peptides were separated using a C18 reversed-phase 100 µm internal diameter × 100 mm analytical column (1.7 µm particle size; BEH130 C18, Waters Co. USA) with an integrated electrospray ionization PicoTip (±10 µm internal diameter; New Objective, USA). The auto-sampler chamber was set to 278 K. The trap, analytical column and all tubing were immersed in an ice bath to minimize deuterium back-exchange. Both mobile-phase bottles were placed on ice and both mobile phases contained 0.1% FA. Gradient chromatography was performed at a flow rate of 600 nl min^{-1} and was sprayed online to a mass spectrometer (SYNAPT HDMS, Waters Co., USA). All mass-spectrometric measurements were taken with capillary voltage 2.5 kV, cone voltage 35 V, extraction cone voltage 4.0 V and source temperature 353 K. A TOF-mode scan was performed in the m/z range 300–1500 with a scan time of 1 s.

2.7. Crystal structure of oxidized Nm23-H1

Details of the crystallization and preliminary X-ray study of oxidized Nm23-H1 have been published elsewhere (Kim *et al.*, 2010). The best cube-shaped crystal of oxidized Nm23-H1 pretreated with 10 m*M* H_2O_2 for 1 h was obtained using a crystallization solution containing 2.0 *M* sodium potassium phosphate pH 6.4, as reported previously. X-ray diffraction data were collected at Pohang Light Source. Initial phases were determined by molecular replacement with *EPMR* (Kissinger *et al.*, 2001) using the crystal structure of native Nm23-H1 (PDB entry 1jxv; Min *et al.*, 2002) as a search model. A dimer composed of two oxidized Nm23-H1 monomers was found in the asymmetric unit. The initial electron-density map was interpretable and was used to fit the protein sequence. A preliminary model was built and refined using the programs *O* (Kleywegt & Jones, 1997), *Coot* (Emsley *et al.*, 2010), *CCP*4 (Winn *et al.*, 2011) and *CNS* (Brünger *et al.*, 1998). Noncrystallographic symmetry (NCS) matrices were obtained for two protomer molecules in the asymmetric unit. NCS restraints were applied during refinement and were released in the final round of refinement. Reflection data between 20.0 and 2.8 Å resolution were included throughout the refinement calculations. 10% of the data were assigned to monitor the free R factor. Isotropic B factors for individual atoms were initially fixed to 20 Å^2 and were refined in the last stages. Final refinement and addition of phosphate ions and water molecules were performed using *CNS* (Brünger *et al.*, 1998) and *PHENIX* (Adams *et al.*, 2010; Afonine *et al.*, 2012). The refinement statistics are shown in Table 1.

2.8. Modelled structures of sulfonylated and glutathionylated Nm23-H1

Energy-minimized models of glutathionylated and sulfonylated Nm23-H1 were obtained using the program *SYBYL-X* 1.3. The sulfonylated model was built and energy-minimized using the Tripos force field with 1000 iterations of Powell's gradient with a distance-dependent dielectric constant equal to 1 and a nonbonded interactions cutoff value of 8, and was terminated at a convergence of 0.5 kcal mol^{-1} Å^{-1}. To obtain an unbiased glutathionylated model, glutathione was docked on the surface around Cys109 (Kellenberger *et al.*, 2004). Prior to docking, H atoms were added to the predicted models using the biopolymer modulators of *SYBYL-X* 1.3. The MMFF94 atom charges were assigned to protein atoms. After running *Surflex-Dock* (Jain, 2007), the scores of the docked conformers were ranked in a molecular spreadsheet. The best-scoring conformer was selected and applied to *Surflex-Dock GeomX*, which uses multiple starting conformations and produces up to 20 docked poses per ligand with a more exhaustive docking-accuracy parameter set. A protein-minimization option or a protein-flexibility option to adapt the active-site conformation to docked ligands was combined with *Surflex-Dock GeomX*. The best pose of glutathionine was used to make a disulfide bridge to Cys109. The same energy-minimization protocol as used for the sulfonylated model was used to obtain the final model of glutathionylated Nm23-H1.

3. Results

3.1. NDPK activity of Nm23-H1 decreases under oxidative stress

To examine whether the oxidation of cysteine residues affects the enzymatic activity of Nm23-H1, the NDPK activity of the wild type and its cysteine mutants (C4S, C109A and C145S) was determined by treating purified recombinant proteins (3 µg) with various concentrations of H_2O_2 in PBS for 1 h at 310 K and measuring their enzymatic activities by separating substrate [γ-^{32}P]ATP and product [γ-^{32}P]UTP on a TLC plate followed by autoradiography. Native Nm23-H1 as well as the C4S and C145S mutants was readily oxidized, with concomitant loss of enzymatic activity. The C4S and C145S mutants were more resistant to oxidative stress than the wild type. The enzymatic activity of the C109A mutant did not decrease (Fig. 2). It exhibited the greatest resistance to oxidative stress among the three cysteine mutants.

3.2. Identification of the cysteine residue oxidized by hydrogen peroxide in Nm23-H1

To identify the cysteine residue involved in oxidative regulation, purified recombinant Nm23-H1 proteins (3 µg) were treated with various concentrations of H_2O_2 for 1 h at 310 K and then treated with 20 m*M* NEM, a thiol-reactive compound commonly used to block the free sulfhydryl group of a cysteine residue, for an additional 10 min to inhibit excessive oxidation of cysteine residues during the experimental procedure. Each sample was separated on a 12% SDS–PAGE gel under nonreducing conditions and stained with Coomassie Blue. As shown in Fig. 3(*a*), Nm23-H1 readily generated a strong intramolecular disulfide bond in response to H_2O_2 treatment. However, the intramolecular disulfide cross-linking was not present in the C4S and C145S mutants. To identify the residues that were crosslinked in oxidized

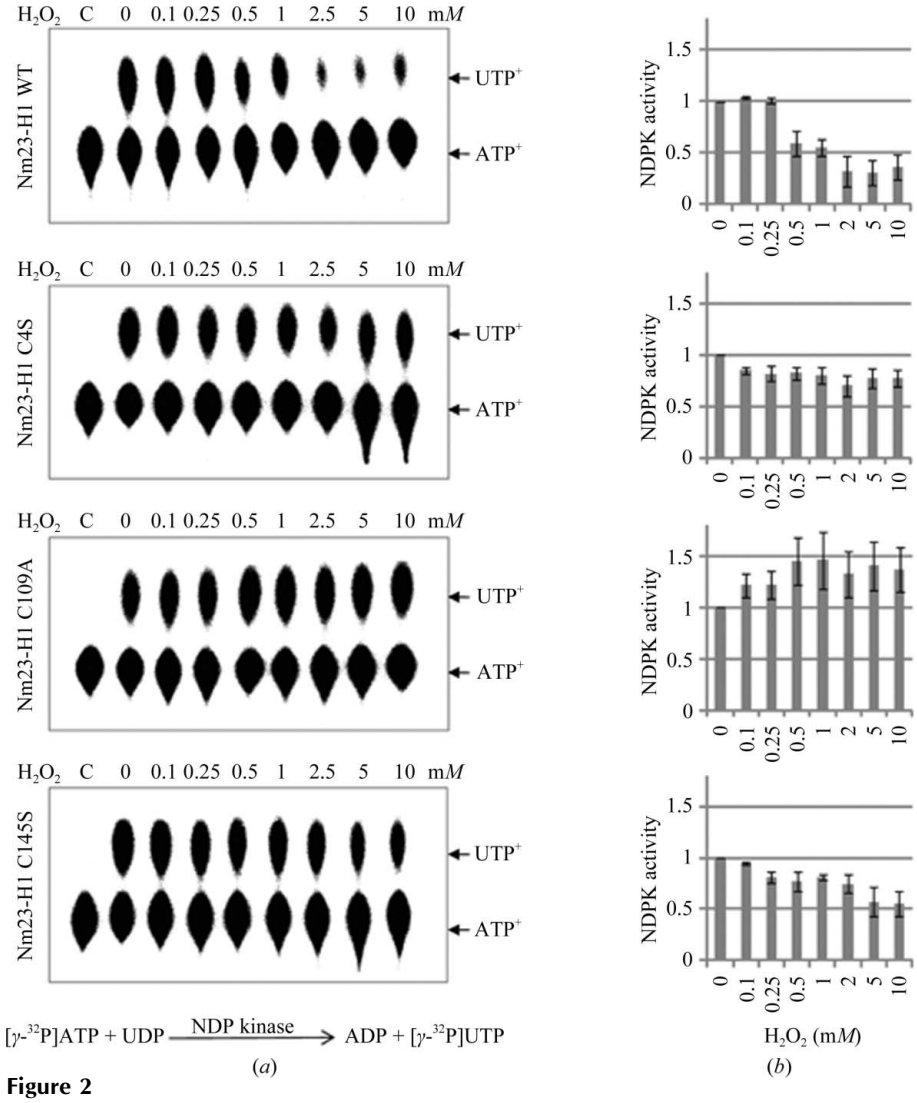

Figure 2
NDPK activities of Nm23-H1 treated with H_2O_2. (*a*) The recombinant proteins were treated with various concentrations of H_2O_2 for 1 h at 310 K and the NDPK activity was measured. (*b*) The presented enzyme-activity values are averages of three independent experiments.

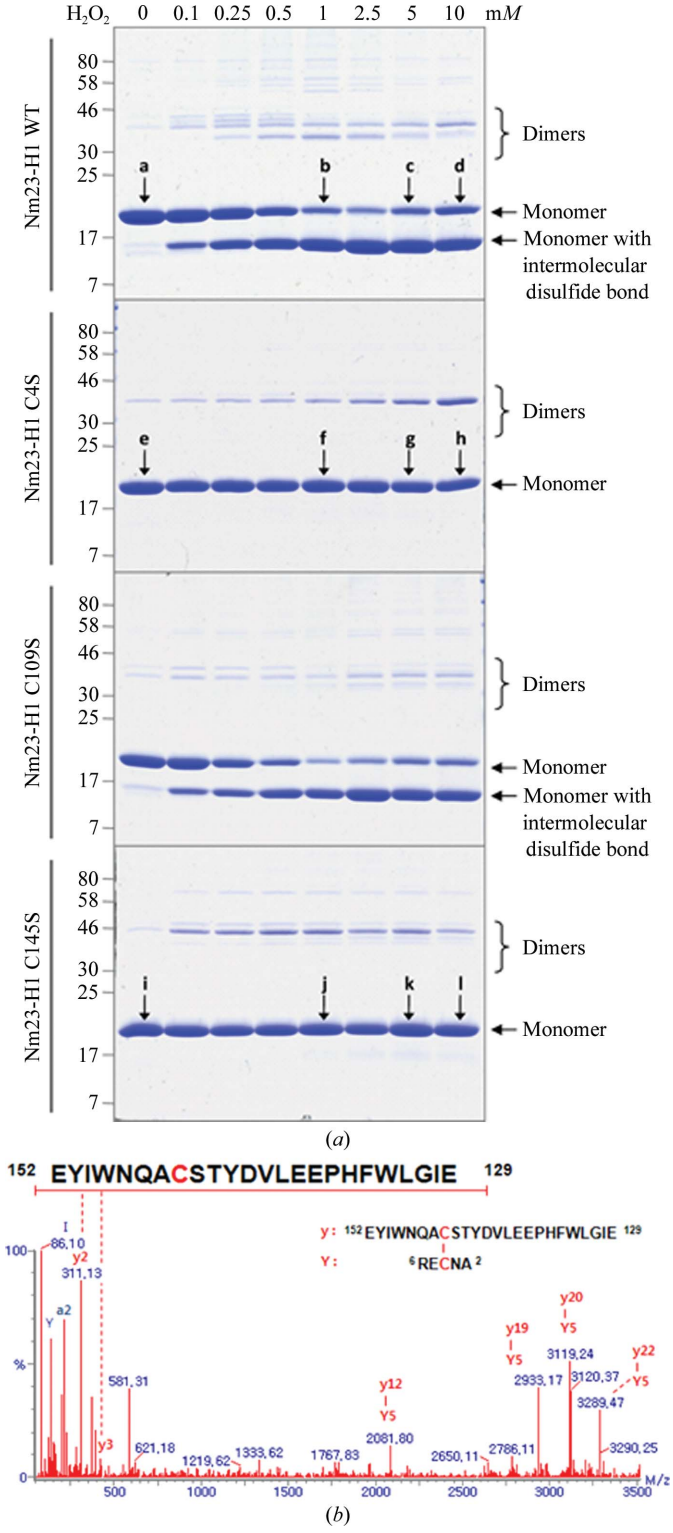

Figure 3
Oxidation patterns of wild-type Nm23-H1 and its cysteine mutants in response to H_2O_2. (*a*) The recombinant proteins were treated with various concentrations of H_2O_2 for 1 h at 310 K and then treated with NEM for an additional 10 min at 310 K. Each reaction product was separated on a 12% SDS–PAGE gel and stained with Coomassie Blue under nonreducing conditions. Intramolecular and intermolecular disulfide-bond formation of Nm23-H1 depends on the H_2O_2 concentration. (*b*) MS/MS spectrum showing the intramolecular disulfide bond between Cys4 and Cys145.

Nm23-H1, peptide sequencing using nanoUPLC-ESI-q-TOF tandem MS was employed in combination with the *DBond* algorithm (Choi *et al.*, 2010) to identify intact disulfide bonds (Fig. 3*b*). We thus identified an intramolecular disulfide bond between Cys4 and Cys145. The population of the intramolecular disulfide bond is proportional to the H_2O_2 concentration for both the wild type and the C109A mutant. However, the C4S and C145S mutants failed to form intramolecular disulfide bonds. This suggests that Cys4 and Cys145 are the key residues that form the intramolecular disulfide cross-links. In order to examine the effect of the intramolecular disulfide bond on the oxidation of Cys109 to sulfonic acid, the degree of oxidation to sulfonic acid was measured by peptide sequencing with nanoUPLC-ESI-q-TOF tandem MS (Figs. 3 and 4). Intriguingly, Cys109 in the wild type was heavily oxidized to sulfonic acid in a H_2O_2 concentration-dependent manner, while

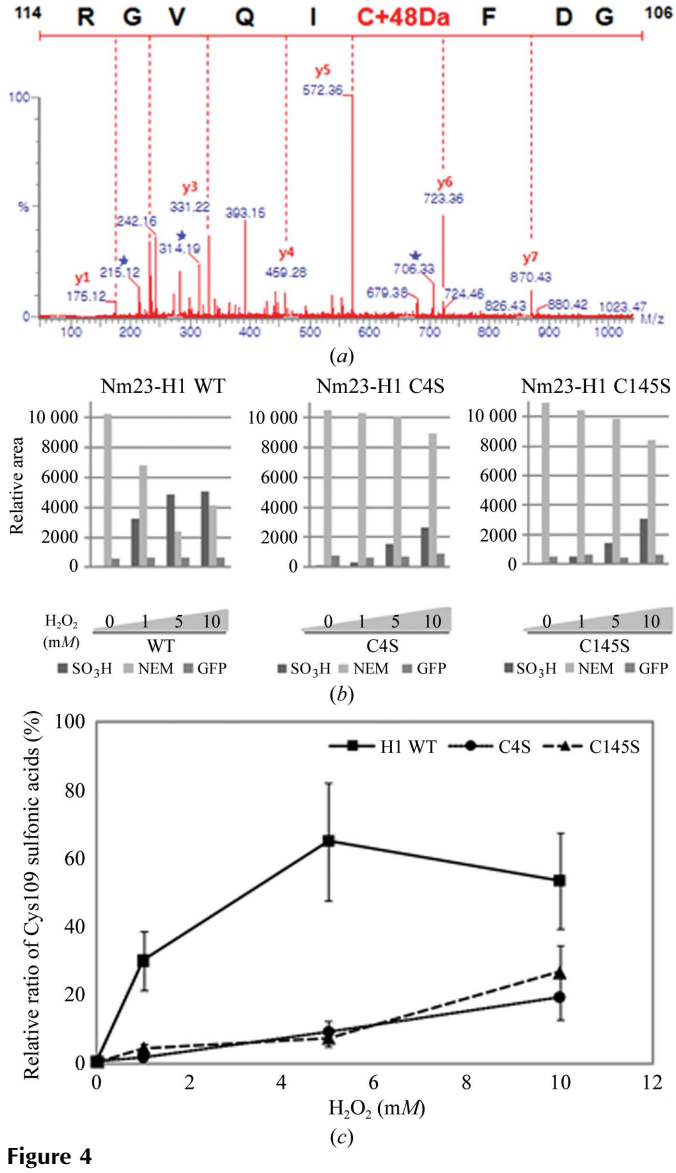

Figure 4
Oxidative modification of wild-type Nm23-H1 and its cysteine mutants at Cys109 in response to H_2O_2. (*a*) MS/MS spectrum showing the sulfonic acid at Cys109. (*b*, *c*) Quantification of the population of sulfonic acid at Cys109 (see §2 for details).

Cys109 in the C4S and C145S mutants was less oxidized to sulfonic acid (Fig. 4). This indicates that formation of the intramolecular disulfide cross-link between Cys4 and Cys145 changes the conformation of Nm23-H1 and induces oxidation of Cys109 to sulfonic acid.

3.3. Characterization of the oligomeric states of redox-sensitive Nm23-H1

To characterize the oligomeric states of redox-sensitive Nm23-H1 subjected to oxidative stimuli, the HDX ratio was monitored using mass spectrometry. HDX was greater in oxidized Nm23-H1 than in the native form (Fig. 5*a* and Supplementary Fig. S1[1]). The HDX ratio of the wild type increased and finally became saturated (Fig. 5*a*). These gradients reflect the influence of H_2O_2 on solvent-accessible surface areas of Nm23-H1, as confirmed by HDX of peptic peptides of oxidized Nm23-H1 (Fig. 5*b*). The peptide containing Cys109 of Nm23-H1 was also exposed to the surface in response to oxidative stimuli (Supplementary Fig. S2). These results indicate that tertiary- and quaternary-structural changes occur in Nm23-H1 in response to oxidative stress.

3.4. Structural analysis of oxidized Nm23-H1

The crystal structure of oxidized Nm23-H1 was determined by molecular replacement using the crystal structure of the native form (PDB entry 1jxv; Min *et al.*, 2002) at 2.8 Å resolution as a model. The final model exhibited appropriate stereochemical geometry and was refined to R and $R_{\rm free}$ values of 19.6 and 24.5%, respectively (Table 1). Owing to the flexibility of the C-terminus, one subunit contains 151 residues and the other contains 149 residues, lacking one and three C-terminal amino acids, respectively. The first methionines in the two subunits were included because the backbone densities were visible in both cases. The weak side-chain density may originate from the natural flexibility of the terminal residue together with possible removal of the N-terminal methinonine from some portion of the Nm23-H1 molecules by methinonine aminopeptidase (MetAP) from *E. coli*. However, the efficiency of MetSA might be seriously reduced owing to the presence of 1 m*M* EDTA, which may extract essential metals for MetSA activity during purification (Chai & Ye, 2009). All residues lie in the allowed regions of the Ramachandran plot produced with *PROCHECK* (Laskowski *et al.*, 1993). Ile116, which is usually located as an outlier in other structures, is found in the allowed region of the Ramachandran plot. This is one result of the influence of the conversion of the preceding loop, which was the 3_{10}-helix G3 in the native structure. Each monomer has a core domain containing a ferrodoxin-like fold and a flexible C-terminal domain (Fig. 6*a*). The six protomers in the unit cell form a triangular structure with a bound phosphate ion in each active site (Figs. 6*a* and 6*b*). The active sites reside on the top and the bottom sides of the structure. Nm23-H1 has at least three known molecular functions conferred by different key residues which are dispersed in the relatively large active-site cleft exposed on the surface without any hindrance from surrounding residues. Glu5 has been shown to be responsible for the 3′–5′ exonuclease activity, Tyr52 and His118 for both the NDPK and histidine kinase activities and Lys12 for all three enzyme activities (Zhang *et al.*, 2011). Interestingly, no prominent conformational change was detected in the active site of the oxidized form except for the distorted backbone of Gly113 influencing the binding affinity of the adenine moiety of ADP (Fig. 6*a*). Some notable changes are found on one side comprising residues 110–116. The effects of flipping of the main chains on conformations are clearly detected. However, the positions of the side chains do not deviate so much from those of the native structure. Although the shift of the positions of side chains Asp14, Arg105, Cys109 and Ile116 are clear, their influence on the active sites may be limited owing

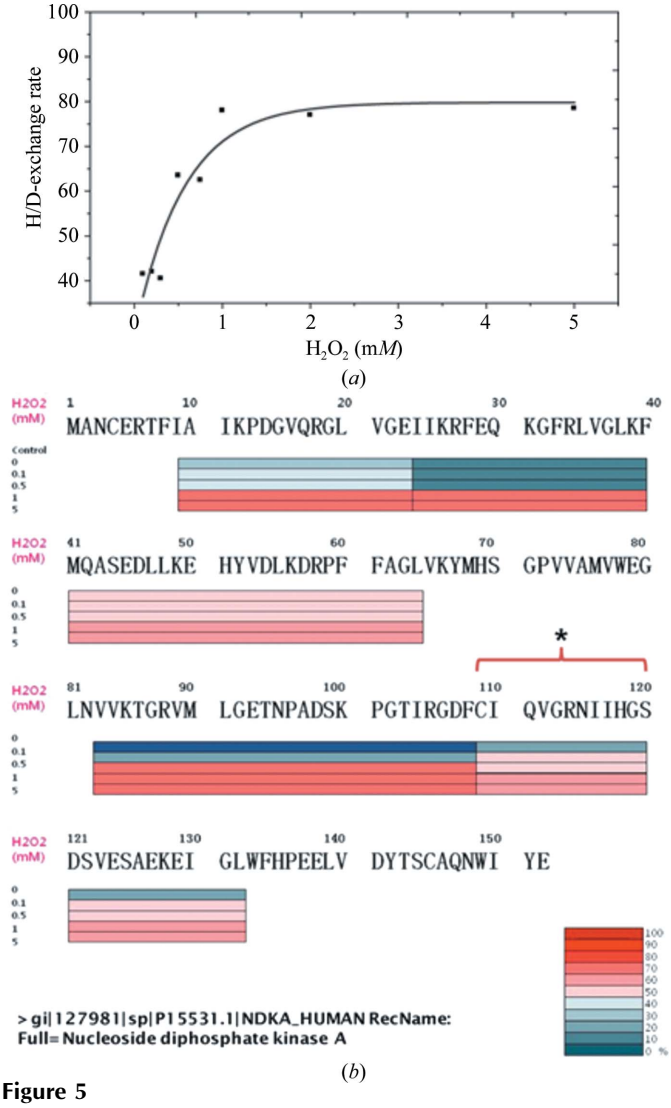

Figure 5
HDX of Nm23-H1. (*a*) HDX ratio of intact Nm23-H1 in response to H_2O_2. (*b*) HDX of peptic peptides of native and oxidized Nm23-H1. The levels of deuteration at residues 109–132 of Nm23-H1 treated with 5 m*M* H_2O_2 and untreated Nm23-H1 are summarized.

[1] Supplementary material has been deposited in the IUCr electronic archive (Reference: MN5019). Services for accessing this material are described at the back of the journal.

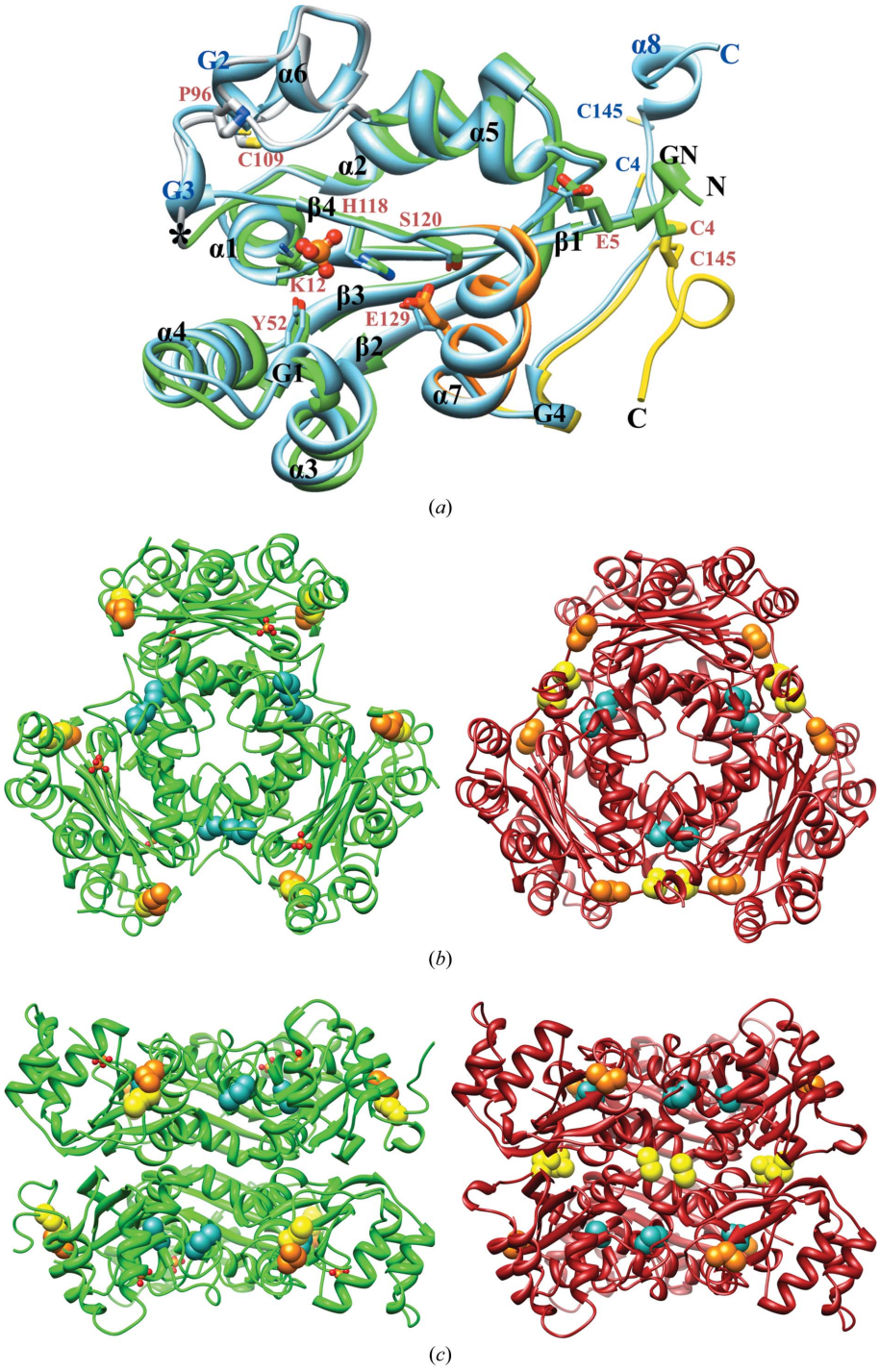

Figure 6
Crystal structure of oxidized Nm23-H1. (*a*) Superposition of monomers of the oxidized and native forms. The native form is coloured cyan. The oxidized form is coloured green, with the K-pn loop region in white, helix H7 (linker helix) in scarlet and the C-terminal domain in yellow. Some of the secondary-structural elements are labelled in blue for the native form and in black for the oxidized form. The phosphate ion and the residues Lys12 and His118 that are essential for NDPK activity form salt bridges with distances of 3.03 and 2.72 Å, respectively. His118, Ser120 and Glu129 form a hydrogen-bond network essential for anchoring the C-terminal domain to the core domain. The distances of the hydrogen bonds His118 $N^{\varepsilon 2}\cdots$Glu129 $O^{\varepsilon 1}$, His118 $N^{\varepsilon 2}\cdots$Glu129 $O^{\varepsilon 2}$ and Ser120 $O^{\gamma}\cdots$Glu129 $O^{\varepsilon 1}$ are 3.01, 3.15 and 2.60 Å, respectively. The residues that interact with ADP are represented and labelled. Gly113 is marked with an asterisk. (*b*) Oxidized (left) and native (right) Nm23-H1 hexamers in crystals. The cysteine residues are represented by spheres: orange for Cys4, cyan for Cys109 and yellow for Cys145. The sulfate molecules are represented as ball-and-stick models. (*c*) This figure was obtained by rotating (*b*) through 90° along the *x* axis.

to their relatively large distance from the substrate-binding site.

However, the architecture of Nm23-H1 along the equatorial surface formed by six protomers is quite different from that of the native structure (Figs. 6*b* and 6*c*). This is caused by the intramolecular disulfide bond between Cys4 and Cys145 that is formed under oxidative conditions. Interestingly, the S^{γ} atoms of the two cysteines are approximately ∼20 Å apart in the native crystal structure. Therefore, an intermolecular disulfide bridge mediated by Cys145 (only ∼5 Å apart in the native form) was expected (Fig. 6*c*) similar to the intermolecular disulfide bridge mediated by Cys133 that stabilizes the tetrameric form of NDPK from *Aquifex aeolicus* (Boissier *et al.*, 2012). The oxidation mechanism of Nm23-H1 may be analogous to that of the atypical 2-Cys peroxiredoxin (Wood *et al.*, 2003). Since Cys4 is predicted to have a lower pK_a than Cys145 using the *Cysteine Oxidation Prediction Algorithm* (*COPA*; Sanchez *et al.*, 2008), Cys4 may be the peroxidatic cysteine that is oxidized first. The sulfhydryl of Cys145 should then be the resolving cysteine.

Biochemical studies using native Nm23-H1 treated with H_2O_2 clearly showed that the intramolecular disulfide-bond population increases proportionally to the H_2O_2 concentration. The protein band that moves faster than the native band on nonreducing SDS–PAGE corresponds to the compact Nm23-H1 formed by the intramolecular disulfide bond. This band is not present for the C4S or C145S mutants, which are not able to form the intramolecular disulfide bond (Fig. 3*a*). The presence of the intramolecular disulfide bond was also confirmed by peptide sequencing using nanoUPLC-ESI-q-TOF tandem MS (Fig. 3*b*).

4. Discussion

Nm23 is known to be involved in several biological processes, including tumour metastasis (Kimura *et al.*, 2000; Leone, Flatow *et al.*, 1993), oncogenesis (Hailat *et al.*, 1991; Leone, Seeger *et al.*, 1993), differentiation (Keim *et al.*, 1992; Ohneda *et al.*, 1994), development

(Biggs *et al.*, 1990; Dearolf, 1998; Timmons *et al.*, 1995; Xu *et al.*, 1996), proliferation (Biggs *et al.*, 1990; Dearolf, 1998; Okabe-Kado *et al.*, 1995; Venturelli *et al.*, 1995) and apoptosis (Venturelli *et al.*, 1995). However, the molecular mechanisms underlying the roles of Nm23 in these processes are not well understood. Our previous studies suggest that Nm23-H1 is involved in the reactive oxygen species (ROS) signalling pathway. Song *et al.* (2000) suggested that disulfide-bond formation in response to H_2O_2 might be a regulatory mechanism of the cellular functions of Nm23-H1. In this study, employing biochemical, X-ray crystallographic and HDX studies of various cysteine mutants of Nm23-H1, we characterized this regulatory mechanism. In the native crystal structure the C-terminal domain of Nm23-H1 wraps around the equatorial surface and thereby stabilizes the hexameric state by interacting with the bottom side of the K-pn loop region of a neighbouring subunit (Supplementary Fig. S3). The surface area of the K-pn loop region covered by the C-terminal domain is $\sim$500 Å^2 per subunit. Under oxidative conditions, the driving force for the formation of the intramolecular disulfide bond induces a large conformational change of the C-terminal domain (Fig. 6). It is triggered by the breakage of two hydrogen bonds between the C-terminal domain and the K-pn loop region (Supplementary Fig. S4*a*). Consequently, a helix-to-loop transition of α8 occurs in the C-terminal domain, which facilitates the $\sim$20 Å movement of Cys145 towards Cys4. This transition also uncovers the bottom side of the K-pn loop region and thereby exposes Cys109 to easy access by solvent molecules (Fig. 6*c*). Cys109 is the key residue susceptible to glutathionylation and is responsible for the deactivation of NDPK under oxidative conditions (Lee *et al.*, 2009). Intriguingly, peptide sequencing using nanoUPLC-ESI-q-TOF tandem MS revealed a sulfonic acid at Cys109 under oxidative conditions (Fig. 3*b*). The degree of oxidative modification of Cys109 to sulfonic acid was measured to assess the effect of exposure of the K-pn loop region. As expected, Cys109 of the wild type was heavily oxidized to sulfonic acid proportionally to the H_2O_2 concentration (Fig. 4), in contrast to Cys109 of the C4S or C145S mutants, which was significantly less oxidized. These results clearly indicate that intramolecular disulfide-bond formation between Cys4 and Cys145 should precede sulfonic acid formation at Cys109. It is noteworthy that sulfonylated Cys109 was not detected, although faint residual electron density corresponding to cysteine sulfenic acid was observed in our oxidized crystal structure. This may result from the tight packing of oxidized Nm23-H1 owing to the high protein concentration in the crystal, as discussed below. As a result, it forms an artificial hexamer and its Cys109 is protected from oxidation by H_2O_2 through the uncovering of the K-pn loop region. Therefore, we suggest that full dissociation from a hexamer into dimers is an obligatory step in generating a sulfonic acid at Cys109.

In order to predict the inactivation mechanism of sulfonic acid at Cys109, an energy-minimized sulfonylated Nm23-H1 model was built using the *SYBYL-X* 1.3 program. The model revealed that the oxygen moiety of the sulfonyl group strongly attracts Arg105 and Asn115. Since the amide moiety of Asn115 is the key residue that holds the phosphate moiety of the nucleotide (Supplementary Fig. S4*b*), the binding affinity of nucleotides to Nm23-H1 is expected to be severely diminished. As a result, the NDPK activity may fully disappear. Since the histidine kinase activity is also dependent on Asn115, we suggest that this activity may also be abolished by a sulfonic acid at Cys109. The NDPK activity of Nm23-H1 is not necessary for its tumour metastasis suppressor activity (Kim *et al.*, 2003). On the other hand, the hexameric state of Nm23-H1 is absolutely required for its tumour metastasis suppressor activity. Studies of P96S and S120G mutants showed that the dimeric form with NDPK activity did not exhibit tumour metastasis suppressor activity. We also observed that dimeric Nm23-H1 is correlated with depression of the metastasis suppressor activity under oxidative conditions (Song *et al.*, 2000; Lee *et al.*, 2009). These results indicate that some of cellular functions of Nm23-H1 may be coupled to its oligomeric states. Three different oligomers of Nm23-H1, namely monomers, dimers and hexamers, have been described. This study found that oxidized Nm23-H1 is a dimer in the asymmetric unit, but that it forms a hexamer in the unit cell in space group $P2_13$. Therefore, we used HDX mass spectrometry to observe conformational dynamics as an alternative approach to demonstrate a transition from a hexamer into monomers under oxidative conditions. Dimeric interfaces (residues 24–40) and the K-pn loop regions (residues 82–108) of Nm23-H1 were detected to show a large difference in HDX ratio depending on the H_2O_2 concentration (Fig. 5). These regions are located at the interfaces of subunits and are blocked from solvent access in the native hexameric structure (Supplementary Fig. S5). As the concentration of H_2O_2 increases, these sites open to solvent in a stepwise manner. At a low concentration of H_2O_2 (above 0.1 m*M* in our data), the K-pn loop region starts to be exposed to solvent. This phenomenon is driven by perturbation of the K-pn loop region triggered by the intramolecular disulfide bridge, as discussed above. This result is consistent with the report on the P96S mutant in which perturbation of the K-pn loop region was proposed to promote the dissociation of a hexamer into dimers (Freije *et al.*, 1997; Kim *et al.*, 2003). We suggest that this dimer formed at low concentrations of H_2O_2 is the biological dimer under oxidative conditions. At high H_2O_2 concentrations (above 0.5 m*M*), the region corresponding to the dimeric interface starts to be exposed and is accessible to solvent. This means that a dimer can be further dissociated into monomers. The presence of a monomeric form was observed for the P96S and S120G mutants (Zhou *et al.*, 2007). However, this monomer may be very unstable owing to the hydrophobic nature of the exposed surface. In summary, Nm23-H1 dissociates from a hexamer into dimers and finally into monomers with increasing H_2O_2 concentration.

The crystal structure of oxidized Nm23-H1 provided an additional insight into its molecular functions. As discussed above, there is almost no conformational change at the active site except for the backbone of Gly113 (Fig. 6*a* and Supplementary Fig. S4*b*), despite the large tertiary and quaternary conformational changes triggered by the intramolecular

disulfide bond. This is in agreement with the report that the P96S and S120G mutants, which are present as dimers in solution, still have NDPK activity (Kim *et al.*, 2003), although some of their activity might be contributed by leftover hexameric Nm23-H1 (Giraud *et al.*, 2006; Mocan *et al.*, 2007). These results indicate that Nm23-H1 recognizes its substrate using a 'lock-and-key' mechanism at the active site regardless of its oligomeric state. In contrast, its tumour metastasis suppressor activity is only exhibited when it exists in the hexameric form with 3′–5′ exonuclease activity (Jarrett *et al.*, 2011). The coupling among the various molecular functions and quaternary conformations of Nm23-H1 may be an efficient way to diversify its cellular functions with at least 20 different binding partners (Marino *et al.*, 2011). In contrast, any mutation influencing the oligomeric state would disturb some of the cellular functions by distorting the binding surfaces for the relevant partner proteins. In the oxidized structure, the backbone geometry of two 3_{10}-helices, G2 and G3, in the K-pn loop region is slightly relaxed and thereby adopts a helical loop conformation (Fig. 6*a*). Since the stable conformation of the K-pn loop region of Nm23-H1 is important for its proper packing to form the functional hexamer, the improper conformation of its K-pn loop region induced by oxidation or mutation seems to accelerate the dissociation of the functional hexamer, as observed in the P96S mutant. The structural role of the proline residue is confirmed by stability studies of wild-type Nm23-H4 to heat and urea treatment, where Ser129 is the native sequence at this position. Substituting proline for serine at this site in the Nm23-H4 mutant clearly increased the structural stability of the wild type (Milon *et al.*, 2000).

The behaviour of the neuroblastoma-associated S120G mutant is also similar to that of the P96S mutant, but uses a different molecular mechanism. Ser120 in the core domain forms a hydrogen bond to Glu129, which also makes a hydrogen bond to His118 (Fig. 6*a*). Since Glu129 is located on the linker helix α7 (Fig. 1), which mediates the anchoring of the C-terminal domain to the core domain, loss of the hydrogen-bond network caused by the S120G mutant would promote flexibility of the C-terminal domain. As a result, the diminished interaction between the C-terminal domain and the K-pn region would accelerate the dissociation of the hexameric state, as observed in the oxidized crystal structure. We confirmed the importance of this hydrogen-bond network in the E129G mutant by observing its denaturation with 5 m*M* H_2O_2 within a day, unlike the wild type. The observation of a molten globule folding intermediate postulated to be involved in amyloidogenic aggregation of the S120G mutant (Georgescauld *et al.*, 2011) is somewhat explicable with our results. The flexibility of the C-terminal domain inducing the quaternary conformational change observed under oxidative conditions would be seriously detrimental if this phenomenon is initiated by certain mutations causing irreversible C-terminal flexibility and is exacerbated by oxidative stress.

Our previous study revealed that Nm23-H1 is regulated by disulfide-bond formation and is easily reduced by the NADPH–TrxR1–Trx system (Lee *et al.*, 2009). In this study, we suggest that Nm23-H1 is regulated by stepwise oxidative modification coupled to its oligomeric state (Fig. 7). After the first oxidation the hexameric Nm23-H1 is dissociated into dimers, triggered by the intramolecular disulfide bond between Cys4 and Cys145. At this point, some of the cellular roles of Nm23-H1 such as its tumour metastasis suppressor activity can be lost (Lee *et al.*, 2009) owing to the deformation of some of the surfaces required for binding partner proteins. However, this dimeric form can acquire other cellular roles by interacting with other partner proteins. It is noteworthy that protein phosphotransferase activity is attributed to the complex of a dimer of glyceraldehyde 3-phosphate dehydrogenase with a dimer of Nm23-H1 (Engel *et al.*, 1998). After the second oxidation, Nm23-H1 loses its NDPK and histidine kinase activities by the formation of a sulfonic acid at Cys109. The second oxidation is only possible when hexameric Nm23-H1 is fully

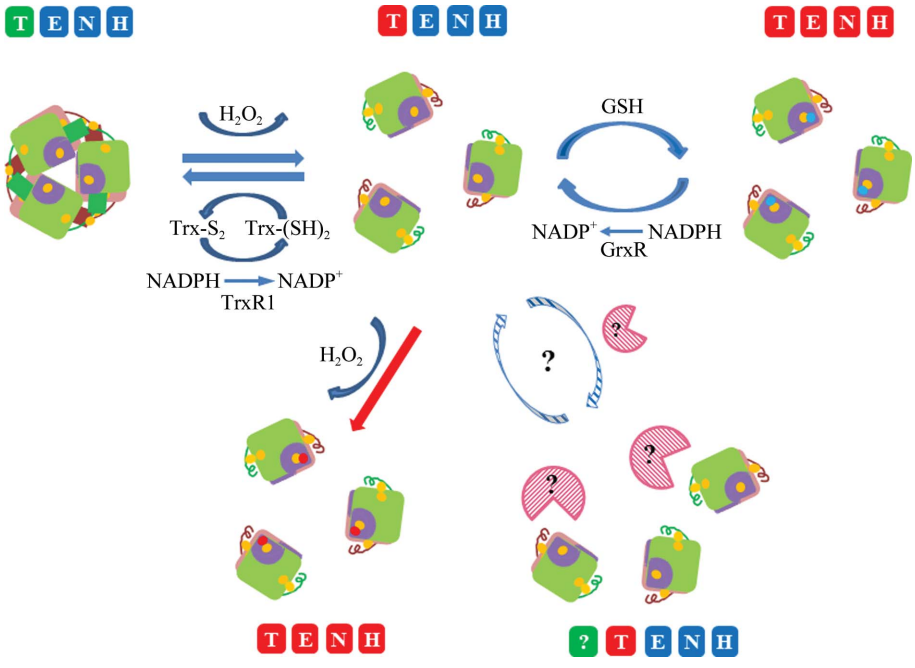

Figure 7
Diagram representing the regulatory mechanism of Nm23-H1 under oxidative conditions. Nm23-H1 is coloured light green or pink, with cysteine residues in yellow, sulfonyl groups in red, glutathione in blue, the K-pn loop region in violet and the C-terminal domain in green or dark red. The green squares represent cellular functions, blue squares molecular functions and red squares inactivated functions. T represents tumour metastasis suppressor activity, E represents 3′–5′ exonuclease activity, N represents NDPK activity, H represents histidine kinase activity and ? represents unknown activity, binding partners and processes. The red arrow indicates the irreversible inactivation process by sulfonylation.

dissociated into dimers. All of the molecular activities of Nm23-H1 are expected to be inhibited by this modification. However, considering Nm23-H1 as a housekeeping enzyme, irreversible oxidative modifications should be avoided. Therefore, we suggest that the cellular role of glutathionylation at Cys109 is to protect Nm23-H1 from irreversible inactivation by sulfonic acid formation under oxidative conditions. The energy-minimized glutathionylated Nm23-H1 model indicates that glutathionylation is only possible in the dimeric state with the aid of two arginine residues: Arg18 and Arg114 (Supplementary Fig. S6). To recover the molecular and cellular functions of Nm23-H1, the thiol state of Cys109 should be restored. This process can be achieved by the NADPH–glutaredoxin reductase–glutaredoxin system in the cell. Reduction of the intramolecular disulfide cross-linking can be performed with the aid of the NADPH–TrxR1–Trx system, as we have shown previously (Lee *et al.*, 2009). As a result, the inactivated Nm23-H1 dimers turn into fully activated hexamers.

In this study, we solved the puzzle of the regulatory mechanism of Nm23-H1 by uncovering the orchestrated oxidative modifications coupled to its oligomeric states through a series of experiments. To our knowledge, this is the first example of regulation of molecular and cellular functions of enzymes through stepwise oxidative modification. Because the number of examples of oxidative modifications is increasing, our findings may be useful to resolve complicated enzyme-regulatory mechanisms operating under oxidative conditions.

We are grateful to the staff of Pohang Light Source for their assistance with synchrotron data collection. This work was supported by the Basic Science Research Program (2011-0005538), the National Core Research Center program (2012-0000952) through the National Research Foundation of Korea grant funded by the Korean Government (MEST) and by the Global Research Lab Program (No. 2012045441) and by the Proteogenomics Research Program (No. 2012036680) through the National Research Foundation of Korea grant funded by the Korean Government (MEST).. Some of the instruments used in this work were granted by Ewha Global Top5 Grant 2011 of Ewha Womans University. M-SK and Jihye Jeong were supported by the Brain Korea 21 (BK21) Project. Author contributions: M-SK, crystallographic studies and manuscript preparation; Jaeho Jeong, biochemical studies and manuscript preparation; Jihye Jeong, proteomic studies using mass spectrometry and manuscript preparation; D-HS, project supervisor, manuscript preparation and principal manuscript author; K-JL, project supervisor, manuscript preparation and principal manuscript author.

References

Adams, P. D. *et al.* (2010). *Acta Cryst.* D**66**, 213–221.
Afonine, P. V., Grosse-Kunstleve, R. W., Echols, N., Headd, J. J., Moriarty, N. W., Mustyakimov, M., Terwilliger, T. C., Urzhumtsev, A., Zwart, P. H. & Adams, P. D. (2012). *Acta Cryst.* D**68**, 352–367.
Arai, S., Yonezawa, Y., Okazaki, N., Matsumoto, F., Tamada, T., Tokunaga, H., Ishibashi, M., Blaber, M., Tokunaga, M. & Kuroki, R. (2012). *Protein Sci.* **21**, 498–510.
Berlett, B. S. & Stadtman, E. R. (1997). *J. Biol. Chem.* **272**, 20313–20316.
Biggs, J., Hersperger, E., Steeg, P. S., Liotta, L. A. & Shearn, A. (1990). *Cell*, **63**, 933–940.
Boissier, F., Georgescauld, F., Moynié, L., Dupuy, J.-W., Sarger, C., Podar, M., Lascu, I., Giraud, M.-F. & Dautant, A. (2012). *Proteins*, **80**, 1658–1668.
Brünger, A. T., Adams, P. D., Clore, G. M., DeLano, W. L., Gros, P., Grosse-Kunstleve, R. W., Jiang, J.-S., Kuszewski, J., Nilges, M., Pannu, N. S., Read, R. J., Rice, L. M., Simonson, T. & Warren, G. L. (1998). *Acta Cryst.* D**54**, 905–921.
Chai, S. C. & Ye, Q.-Z. (2009). *BMC Biochem.* **10**, 32.
Chen, Y., Gallois-Montbrun, S., Schneider, B., Véron, M., Moréra, S., Deville-Bonne, D. & Janin, J. (2003). *J. Mol. Biol.* **332**, 915–926.
Choi, S., Jeong, J., Na, S., Lee, H. S., Kim, H-Y., Lee, K-J. & Paek, E. (2010). *J. Proteome Res.* **9**, 626–635.
Choi, H., Kim, S., Mukhopadhyay, P., Cho, S., Woo, J., Storz, G. & Ryu, S. E. (2001). *Cell*, **105**, 103–113.
Dearolf, C. R. (1998). *Biochim. Biophys. Acta*, **1377**, M13–M23.
Emsley, P., Lohkamp, B., Scott, W. G. & Cowtan, K. (2010). *Acta Cryst.* D**66**, 486–501.
Engel, M., Seifert, M., Theisinger, B., Seyfert, U. & Welter, C. (1998). *J. Biol. Chem.* **273**, 20058–20065.
Freije, J. M. P., Blay, P., MacDonald, N. J., Manrow, R. E. & Steeg, P. S. (1997). *J. Biol. Chem.* **272**, 5525–5532.
Fu, X., Kassim, S. Y., Parks, W. C. & Heinecke, J. W. (2001). *J. Biol. Chem.* **276**, 41279–41287.
Georgescauld, F., Sabaté, R., Espargaró, A., Ventura, S., Chaignepain, S., Lacombe, M. & Lascu, I. (2011). *Naunyn Schmiedebergs Arch. Pharmacol.* **384**, 373–381.
Giraud, M.-F., Georgescauld, F., Lascu, I. & Dautant, A. (2006). *J. Bioenerg. Biomembr.* **38**, 261–264.
Hailat, N., Keim, D. R., Melhem, R. F., Zhu, X., Eckerskorn, C., Brodeur, G. M., Reynolds, C. P., Seeger, R. C., Lottspeich, F., Strahler, J. R. & Hanash, S. M. (1991). *J. Clin. Invest.* **88**, 341–345.
Hall, A., Karplus, P. A. & Poole, L. B. (2009). *FEBS J.* **276**, 2469–2477.
Han, B., Min, K., Lee, B. & Lee, S. (2010). *Bull. Korean Chem. Soc.* **31**, 1397–1399.
Hoofnagle, A. N., Resing, K. A. & Ahn, N. G. (2004). *Methods Mol. Biol.* **250**, 283–298.
Ishikawa, N., Shimada, N., Takagi, Y., Ishijima, Y., Fukuda, M. & Kimura, N. (2003). *J. Bioenerg. Biomembr.* **35**, 7–18.
Jain, A. N. (2007). *J. Comput. Aided Mol. Des.* **21**, 281–306.
Janda, I., Devedjiev, Y., Derewenda, U., Dauter, Z., Bielnicki, J., Cooper, D. R., Graf, P. C., Joachimiak, A., Jakob, U. & Derewenda, Z. S. (2004). *Structure*, **12**, 1901–1907.
Jarrett, S. G., Novak, M., Dabernat, S., Daniel, J. Y., Mellon, I., Zhang, Q., Harris, N., Ciesielski, M. J., Fenstermaker, R. A., Kovacic, D., Slominski, A. & Kaetzel, D. M. (2011). *Cancer Res.* **72**, 133–143.
Keim, D., Hailat, N., Melhem, R., Zhu, X., Lascu, I., Veron, M., Strahler, J. & Hanash, S. M. (1992). *J. Clin. Invest.* **89**, 919–924.
Kellenberger, E., Rodrigo, J., Muller, P. & Rognan, D. (2004). *Proteins*, **57**, 225–242.
Kim, M.-S., Jeong, J., Lee, K.-J. & Shin, D. H. (2010). *Acta Cryst.* F**66**, 1490–1492.
Kim, S., Na, S., Sim, J. W., Park, H., Jeong, J., Kim, H., Seo, Y., Seo, J., Lee, K.-J. & Paek, E. (2006). *Nucleic Acids Res.* **34**, W258–W263.
Kim, S. Y., Chang, K. H., Doh, H. J., Jung, J. A., Kim, E., Sim, C. J. & Lee, K.-J. (1997). *Mol. Cells*, **7**, 630–634.
Kim, Y.-I., Park, S., Jeoung, D.-I. & Lee, H. (2003). *Biochem. Biophys. Res. Commun.* **307**, 281–289.
Kimura, N., Shimada, N., Fukuda, M., Ishijima, Y., Miyazaki, H., Ishii, A., Takagi, Y. & Ishikawa, N. (2000). *J. Bioenerg. Biomembr.* **32**, 309–315.

Kissinger, C. R., Gehlhaar, D. K., Smith, B. A. & Bouzida, D. (2001). *Acta Cryst.* D**57**, 1474–1479.
Kleywegt, G. J. & Jones, T. A. (1997). *Methods Enzymol.* **277**, 208–230.
Laskowski, R. A., MacArthur, M. W., Moss, D. S. & Thornton, J. M. (1993). *J. Appl. Cryst.* **26**, 283–291.
Lee, E., Jeong, J., Kim, S. E., Song, E. J., Kang, S. W. & Lee, K.-J. (2009). *PLoS One*, **4**, e7949.
Leone, A., Flatow, U., VanHoutte, K. & Steeg, P. (1993). *Oncogene*, **8**, 2325–2333.
Leone, A., Seeger, R., Hong, C., Hu, Y., Arboleda, M., Brodeur, G., Stram, D., Slamon, D. & Steeg, P. (1993). *Oncogene*, **8**, 855–865.
Marino, N., Marshall, J. & Steeg, P. S. (2011). *Naunyn Schmiedebergs Arch. Pharmacol.* **384**, 351–362.
Milon, L., Meyer, P., Chiadmi, M., Munier, A., Johansson, M., Karlsson, A., Lascu, I., Capeau, J., Janin, J. & Lacombe, M.-L. (2000). *J. Biol. Chem.* **275**, 14264–14272.
Min, K., Song, H. K., Chang, C., Kim, S. Y., Lee, K.-J. & Suh, S. W. (2002). *Proteins*, **46**, 340–342.
Mocan, I., Georgescauld, F., Gonin, P., Thoraval, D., Cervoni, L., Giartosio, A., Dabernat-Arnaud, S., Crouzet, M., Lacombe, M. L. & Lascu, I. (2007). *Biochem. J.* **403**, 149–156.
Montfort, R. L. van, Congreve, M., Tisi, D., Carr, R. & Jhoti, H. (2003). *Nature (London)*, **423**, 773–777.
Moréra, S., LeBras, G., Lascu, I., Lacombe, M.-L., Véron, M. & Janin, J. (1994). *J. Mol. Biol.* **243**, 873–890.
Moynié, L., Giraud, M.-F., Georgescauld, F., Lascu, I. & Dautant, A. (2007). *Proteins*, **67**, 755–765.
Na, S., Jeong, J., Park, H., Lee, K.-J. & Paek, E. (2008). *Mol. Cell. Proteomics*, **7**, 2452–2463.
Nagashima, S., Nakasako, M., Dohmae, N., Tsujimura, M., Takio, K., Odaka, M., Yohda, M., Kamiya, N. & Endo, I. (1998). *Nature Struct. Biol.* **5**, 347–351.
Ohneda, K., Fukuda, M., Shimada, N., Ishikawa, N., Ichou, T., Kaji, K., Toyota, T. & Kimura, N. (1994). *FEBS Lett.* **348**, 273–277.
Okabe-Kado, J., Kasukabe, T., Baba, H., Urano, T., Shiku, H. & Honma, Y. (1995). *Biochim. Biophys. Acta*, **1267**, 101–106.
Reddie, K. G. & Carroll, K. S. (2008). *Curr. Opin. Chem. Biol.* **12**, 746–754.
Sanchez, R., Riddle, M., Woo, J. & Momand, J. (2008). *Protein Sci.* **17**, 473–481.
Seo, J., Jeong, J., Kim, Y. M., Hwang, N., Paek, E. & Lee, K.-J. (2008). *J. Proteome Res.* **7**, 587–602.
Seyedarabi, A., Sullivan, J. A., Sasakawa, C. & Pickersgill, R. W. (2010). *FEBS Lett.* **584**, 4163–4168.
Song, E. J., Kim, Y. S., Chung, J. Y., Kim, E., Chae, S.-K. & Lee, K.-J. (2000). *Biochemistry*, **39**, 10090–10097.
Strelkov, S. V., Perisic, O., Webb, P. A. & Williams, R. L. (1995). *J. Mol. Biol.* **249**, 665–674.
Timmons, L., Xu, J., Hersperger, G., Deng, X. F. & Shearn, A. (1995). *J. Biol. Chem.* **270**, 23021–23030.
Venturelli, D., Martinez, R., Melotti, P., Casella, I., Peschle, C., Cucco, C., Spampinato, G., Darzynkiewicz, Z. & Calabretta, B. (1995). *Proc. Natl Acad. Sci. USA*, **92**, 7435–7439.
Wagner, P. D. & Vu, N. D. (1995). *J. Biol. Chem.* **270**, 21758–21764.
Waterhouse, A. M., Procter, J. B., Martin, D. M., Clamp, M. & Barton, G. J. (2009). *Bioinformatics*, **25**, 1189–1191.
Winn, M. D. *et al.* (2011). *Acta Cryst.* D**67**, 235–242.
Wood, Z. A., Schröder, E., Harris, J. R. & Poole, L. B. (2003). *Trends Biochem. Sci.* **28**, 32–40.
Xu, J., Liu, L. Z., Deng, X. F., Timmons, L., Hersperger, E., Steeg, P. S., Veron, M. & Shearn, A. (1996). *Dev. Biol.* **177**, 544–557.
Zdanowski, K., Doughty, P., Jakimowicz, P., O'Hara, L., Buttner, M. J., Paget, M. S. & Kleanthous, C. (2006). *Biochemistry*, **45**, 8294–8300.
Zhang, Q., McCorkle, J. R., Novak, M., Yang, M. & Kaetzel, D. M. (2011). *Int. J. Cancer*, **128**, 40–50.
Zhou, Q., Yang, X., Zhu, D., Ma, L., Zhu, W., Sun, Z. & Yang, Q. (2007). *Biochem. Biophys. Res. Commun.* **356**, 348–353.